Authors' Accepted Manuscript : Journal of Physics D: Applied Physics, 48 , 015103 (2015).

Composition, structure and morphology of $Al_{1-x}In_xN$ thin films grown on $Al_{1-y}Ga_yN$ templates with different GaN contents

S. Magalhães[1,2,3], I. M. Watson[4], S. Pereira[5], N. Franco[1], L. T. Tan[6]*, R. W. Martin[6], K. P. O'Donnell[6], E. Alves[1], J. P. Araújo[3], T. Monteiro[2], K. Lorenz[1]

[1] IPFN, Instituto Superior Técnico, Campus Tecnológico e Nuclear, 2696-953 Sacavém, Portugal

[2] Departamento de Física and i3N, Universidade de Aveiro, Campus de Santiago, 3810-193 Aveiro, Portugal

[3] IFIMUP/IN, Instituto de Física dos Materiais da Faculdade de Ciência da Universidade do Porto, Instituto de Nanociência e Nanotecnologia, Rua do Campo Alegre, 687 4169-007 Porto, Portugal

[4] Institute of Photonics, Department of Physics, SUPA, University of Strathclyde, Glasgow, G4 0NW, UK

[5] CICECO, Departamento de Física, Universidade de Aveiro, 3810-193 Aveiro, Portugal

[6] Department of Physics, SUPA, University of Strathclyde, Glasgow, G4 0NG, Scotland, UK

Abstract

Four $Al_{1-x}In_xN$ thin films were grown simultaneously on $Al_{1-y}Ga_yN$ (y=1, 0.93, 0.86, and 0.69) buffer layers by Metal Organic Chemical Vapour Deposition (MOCVD). A nominal InN content of ~16% was chosen to achieve closely lattice matched $Al_{1-x}In_xN$ on the buffer layers with intermediate GaN molar fractions, a small tensile strain for growth on GaN, and compressive strain for the buffer layer with the lowest GaN fraction. Only the film deposited on GaN shows true pseudomorphic growth to the template; this film also reveals the highest structural quality, the lowest surface roughness and a homogeneous composition with depth. For growth on the ternary templates, the film roughness and the surface pit density both increase with decreasing GaN content of the $Al_{1-y}Ga_yN$ template, in line with the roughening of the growth templates themselves. Detailed study indicates that the structural and morphological qualities of the templates influence not only the structure and morphology of the films but also their phase homogeneity. Surface roughness of the template is implicated in the formation of V-pits which lead to phase separation due to a decreased incorporation of In on their inclined facets.

1. Introduction

The wide and direct band gap wurtzite III-nitride semiconductors are suitable materials for light emitting diodes (LEDs), lasers as well as high power, high frequency and high temperature electronic devices [1]. The binary semiconductors AlN, GaN and InN can be alloyed to ternary or quaternary compounds opening the possibility to tune the bandgap between 0.7 eV (InN) and 6.2 eV (AlN). Most realized devices are based on $In_yGa_{1-y}N$ or $Al_{1-y}Ga_yN$ ternaries. However, there is a large lattice mismatch between the three binary compounds. Heterostructures,

*Current address: School of Engineering, Republic Polytechnic, 9 Woodlands Ave 9, Singapore 738964

usually consisting of several different binary and ternary layers, suffer from large strains which can lead for example to cracking, the formation of misfit dislocations, and compositional inhomogeneity e.g. due to "compositional pulling" [2-5].

$Al_{1-x}In_xN$ semiconductor alloys are attracting much research interest due to the possibility of lattice matching them to GaN buffer layers [6]. According to Vegard's rule [7], the lattice match condition of an $Al_{1-x}In_xN$ film grown on top of a GaN template would occur at an InN content of approximately 17-18% (depending on the exact *a* lattice parameter of the GaN buffer layer). At this $Al_{1-x}In_xN$ composition, defects associated with lattice mismatch are expected to decrease and device efficiency to increase. The near-lattice-match conditions between $Al_{1-x}In_xN$ and GaN are suitable for the development and fabrication of Bragg mirrors and microcavities [6] and high electron mobility transistors [8,9] in the fields of optoelectronics and microelectronics, respectively. High quality near-lattice-matched $Al_{1-x}In_xN$/GaN bilayers, reported by several research groups, were mostly grown by Metal Organic Chemical Vapour Deposition (MOCVD) or molecular beam epitaxy (MBE) [8-15].

Growing $Al_{1-x}In_xN$ on $Al_{1-y}Ga_yN$ buffer layers further increases the possibilities to achieve lattice-matching conditions since for certain composition pairs (x,y) $Al_{1-x}In_xN$ alloys are lattice-matched to $Al_{1-y}Ga_yN$ buffer layers while exhibiting different band gaps and refractive indices. In particular, this has been exploited for the crack-free growth of $Al_{0.85}In_{0.15}N/Al_{0.2}Ga_{0.8}N$ distributed Bragg reflectors [16].

$Al_{1-x}In_xN$ growth is very challenging due to the large thermal and size mismatches of the binaries AlN and InN. The purpose of this work is to study the structural and morphological properties of $Al_{1-x}In_xN$ thin films grown on $Al_{1-y}Ga_yN$ buffer layers with different GaN contents. It is shown that growth of good quality $Al_{1-x}In_xN$ on $Al_{1-y}Ga_yN$ buffer layers is possible; however, special attention needs to be paid to improving the quality and in particular the morphology of the buffer layers which is shown to strongly influence the $Al_{1-x}In_xN$ growth process.

2. Experimental details

2.1 Sample growth

The GaN/sapphire template (sample A), ~1 µm thick, was grown by MOCVD. The ~0.5-0.9 µm thick ternary $Al_{1-y}Ga_yN$/sapphire templates with different GaN contents [y=0.93 (sample B), 0.86 (sample C) and 0.69 (sample D)], purchased from TDI (Oxford Instruments), were grown by Hydride Vapour Phase Epitaxy (HVPE). All these templates were grown on 2-inch (0001) sapphire substrates with similar thickness and were cut into quarters of quadrant shape using a precision saw, allowing assembly of four quarters in the 2-inch substrate holder of an Aixtron 200-series horizontal flow MOCVD reactor. $Al_{1-x}In_xN$ was grown simultaneously on these four quarter wafers, one of each template, while rotating the substrate holder about a vertical axis running through the vertices of the quadrants. Close packing was important to minimise perturbations of growth conditions at the edges of each quadrant, and the maximum lateral gaps between their straight edges during growth are estimated as ~0.3 mm. Prior to the film growth the samples were cleaned in 18% hydrochloric acid before loading into the reactor and then heated under an ammonia-hydrogen ambient to a set point of 1070 °C with a holding time of 30 seconds in order to clean the surface and remove any oxide layer. The $Al_{1-x}In_xN$ growth was then directly performed on the template without any intermediate buffer layers

using similar conditions as in ref. [3]. The $Al_{1-x}In_xN$ growth setpoint temperature was 790 °C with a growth time of 100 min yielding layer thicknesses of approximately 110 nm. The growth was performed using a N_2 pressure of 75 mbar, with trimethylaluminium and trimethylindium precursor flow rates of 55 and 35 µmol/min, respectively. The V/III ratio was 2480 using ammonia as the nitrogen source.

Samples for the measurements were cut as a rectangular strip from one straight edge of each quarter wafer. In later references to the centre, middle and edge of individual samples, the centre refers to the end of the strip closest to the rotation axis of the MOCVD substrate holder.

2.2 Characterization techniques

The templates and $Al_{1-x}In_xN$ samples were analysed using X-Ray Diffraction (XRD), Rutherford Backscattering Spectrometry/Ion channelling (RBS/C), Atomic Force Microscopy (AFM) and Scanning Electron Microscopy (SEM).
For the XRD measurements, performed on a Bruker D8 AXS diffractometer, the Cu $K_{\alpha 1}$ line was selected using a 2-bounce Ge (220) monochromator and a Göbel mirror. To decrease the horizontal angular divergence, a 0.2 mm wide slit was placed between the Göbel mirror and the monochromator. Asymmetric reciprocal space maps (RSMs) were acquired using a 0.1 mm wide slit placed in front of a scintillation detector and probing the entire length of the sample strip. Rocking curves (RC) were acquired using the open detector.
RBS/C measurements were performed on a Van de Graaff accelerator using 1.2 MeV and 2 MeV He^+ particles for composition and crystal quality characterization, respectively, and a p-*i*-n diode detector, placed at 165° backscattering angle, to collect the backscattered particles. Random spectra and spectra aligned along the c-axis and the $<\bar{2}113>$ axis were acquired. Random spectra were analysed using the NDF fitting code [17].
Atomic Force Microscopy (AFM) measurements were performed using tapping mode on a DI Nanoscope, type IIIa. Surface roughness values were determined in an area of $5x5\mu m^2$. Secondary electron images were obtained using a FEI Sirion scanning electron microscope.

3. Results and discussion

3.1 Compositional analysis and strain

The compositional analysis of the $Al_{1-y}Ga_yN$ and $Al_{1-x}In_xN$ films was performed by XRD and RBS. $Al_{1-y}Ga_yN$ *a* and *c* lattice parameters were determined using Bond's method [18] acquiring $(10\bar{1}4)$ asymmetric and (0004) symmetric XRD RCs. The lattice parameters of the $Al_{1-x}In_xN$ films were then determined using $(10\bar{1}5)$ RSMs. The composition of the ternaries was calculated using Vegard's rule [7]. Biaxial strain was taken into account using Poisson's equation. The relaxed a_0 and c_0 lattice parameters of AlN, GaN and InN and respective C_{13} and C_{33} stiffness coefficients used in this work are listed in Table I. Note that deviations of lattice parameters and stiffness constants for III-N alloys from Vegard's rule are still under discussion but are negligible for the conclusions of this paper [10,24,25]. The determined values of the lattice parameters of the templates, as well as the derived compositions, and strain states are

summarized in Table II. The calculated lattice parameters of relaxed $Al_{1-y}Ga_yN$ alloys with the same composition are also given in Table II. It is found that the ternary $Al_{1-y}Ga_yN$ templates are basically relaxed and that, as expected, the in-plane *a* lattice parameter decreases with decreasing GaN content.

Next, for each $Al_{1-y}Ga_yN$ template we determined the required composition to achieve lattice matched $Al_{1-x}In_xN$ films yielding x = 0.173 (film A), 0.154 (film B), 0.157 (film C), 0.130 (film D) for y = 1 (template A), 0.929 (template B), 0.864 (template C), 0.691 (template D), respectively. The nominal InN content for the simultaneous growth of the films was therefore chosen to be x~0.16 in order to achieve close lattice matches for the two intermediate $Al_{1-y}Ga_yN$ compositions (films B and C).

The XRD $(10\bar{1}5)$ RSMs are shown in Figs. 1a)-d) for the four $Al_{1-x}In_xN/Al_{1-y}Ga_yN$ samples. The $Al_{1-y}Ga_yN$ Q_z $(10\bar{1}5)$ reciprocal lattice units are increasing from figure 1a) to figure 1d) corresponding to a decrease of the $Al_{1-y}Ga_yN$ *c*-lattice parameter with decreasing GaN content. Table II summarizes the measured $Al_{1-x}In_xN$ *a* and *c* lattice parameters found by fitting horizontal and vertical cuts through the RSMs. The error in the lattice parameters given in Table II are found by adding in quadrature an error in the lattice parameters of $Al_{1-y}Ga_yN$ derived from the Bond method and an error in finding the maximum of the $Al_{1-x}In_xN$ peak in the RSM. The latter was found to be the larger factor. The uncertainties in the lattice parameters of film D are much higher than in the other films due to the partial overlap of the Bragg peaks of film and template.

The average $Al_{1-x}In_xN$ compositions derived from RSM (see Table II and Figs. 1a-d) are close to the targeted value of 16 %. However, despite the films' simultaneous growth, the InN molar fraction is not exactly the same in the four films. Jiao et al. [26] proposed, on the basis of the model of Zhu et al. [27], that tensile strain should facilitate the incorporation of In while compressive strain should hinder it, since the impurity formation energy should decrease monotonically when the host lattice is strained in the same direction as the volume change induced by the substituent atom. Following this model, the InN molar faction x in our films should increase with the GaN content y of the growth template; however, no monotonic relationship between x and y is found. The horizontal lines Q_z=61.62 nm^{-1}, Q_z=61.78 nm^{-1} and Q_z=61.59 nm^{-1} in figure 1b, c and d, respectively, mark the Q_z values calculated assuming that films B ($Al_{0.833}In_{0.167}N$), C ($Al_{0.845}In_{0.155}N$) and D ($Al_{0.831}In_{0.169}N$) have the same *a*-parameter as that of film A ($Al_{0.835}In_{0.165}N$), i.e., a=3.186 Å, in order to allow a visual comparison of these Q_z values despite the different in-plane lattice constants of the four templates.

We have shown previously that the growth temperature has a strong effect on the incorporation of InN in $Al_{1-x}In_xN$ films with an approximately linear decrease of InN content with increasing growth temperature [3,10,28]. The compositional differences may therefore be due to a slightly different thermal contact of the four different templates, associated with curvature at the growth temperature. Also the gas fluxes during growth may be slightly disturbed at the junctions between the four quarter wafers and, in fact, lateral compositional gradients also exist in the samples, which are likely also correlated with curvature-induced variations in thermal contact. However, and more importantly, RBS spectra (Fig. 2) reveal compositional gradients with depth in some of the samples as seen in the In-signal between channels ~600 and 750. The InN content increases with depth towards the interface with the $Al_{1-y}Ga_yN$ buffer layer by ~1%, ~5% and ~5% for samples B, C and D, respectively; while the film

grown on GaN reveals a homogeneous InN distribution with depth. These gradients are not resolved in the XRD data due to the strong broadening of the peaks.
Compositional gradients have often been observed in samples that show strain relaxation with depth [3,26,28]. The RSMs in Fig. 1 reveal, that only the $Al_{1-x}In_xN$ film grown on GaN is completely pseudomorphic. The layers grown on ternary templates reveal slightly different *a*-lattice parameters for films and templates. The high symmetry of the reflections for $Al_{1-x}In_xN$ suggests that the films are homogeneously strained without pronounced relaxation during the film growth. The strain state is probably assumed during the nucleation process within a very thin layer and then stays constant, as expected for close to lattice-matched films. The strain state of the $Al_{1-x}In_xN$ films and their $Al_{1-y}Ga_yN$ templates are summarized in table III. The $Al_{1-x}In_xN$ film grown on GaN is under full, tensile, strain. The $Al_{1-x}In_xN$ layers grown on the ternary $Al_{1-y}Ga_yN$ templates are compressively strained with the exception of film C ($Al_{0.845}In_{0.155}N$) which reveals tensile strain. In fact, lattice parameter measurements were performed along the entire strip of sample C and tensile strain was identified in each single analysed spot (not shown) although the combination of the composition of the film and the *a*-lattice parameter of the template should impose lattice-matched growth. Such stresses may be introduced during crystallite coalescence and grain boundary formation in the initial stages of growth [29] and similar observations have been made for $Al_{1-x}In_xN$ grown on GaN by molecular beam epitaxy [30].

3.2 Crystal quality, lateral homogeneity and morphology

Figure 3 a) shows 2 MeV He^+ random and <0001> aligned RBS/C spectra of template B ($Al_{0.071}Ga_{0.929}N$) acquired at three different sample spots corresponding to the wafer centre, middle of the sample strip and wafer edge.

The random spectra taken in three different points of the template do not overlap completely (Fig. 3 a) showing that the $Al_{1-y}Ga_yN$ alloy composition changes slightly laterally and in-depth. The crystal quality, on the other hand, is homogeneous and very good with <0001> minimum yields between 2 and 2.4%. The minimum yield, χ_{min}, is defined by the ratio of the backscattering yield in the aligned spectrum to that in the random spectrum, and it is a measure of the crystal quality [4]. It is determined in a depth region close to the surface. Similar χ_{min} values and good homogeneity are found for all templates as summarized in Table III (1.7% for GaN and 2.1-2.9% for $Al_{1-y}Ga_yN$ for the growth direction and 2.7% for GaN and 6- 8% for $Al_{1-y}Ga_yN$ for the <$\bar{2}$113> axis (spectra not shown)). Along the <$\bar{2}$113> axis the χ_{min} of Ga is more than twice as large for the ternary $Al_{1-y}Ga_yN$ templates than for GaN suggesting higher twist in the ternary $Al_{1-y}Ga_yN$ templates.
Fig. 3 b) shows the RBS/C spectra of sample B ($Al_{0.833}In_{0.167}N/Al_{0.071}Ga_{0.929}N$) after the $Al_{1-x}In_xN$ growth on the template shown in Fig. 3 a). In contrast to the template, the In <0001> minimum yield is seen to vary strongly between different points of the sample: it increases towards the edge of the wafer. The same is seen for film D ($Al_{0.831}In_{0.169}N$) while for film C ($Al_{0.845}In_{0.155}N$), the <0001> minimum yield decreases slightly towards the edge of the sample (χ_{min}(In,centre)=11.6%; χ_{min}(In,edge)=10.4%, see table III). Minimum yields for the films grown on ternary $Al_{1-y}Ga_yN$ vary between ~6% and ~22% for the <0001> axis and between 8% and 37% for the <$\bar{2}$113> axis. These values still reveal good crystal quality for a ternary but

represent poorer quality than the growth templates. Furthermore, the best values of ~4% along <0001> throughout the wafer are found for the film grown on GaN.

By definition, a high In minimum yield reveals a high fraction of In atoms displaced from substitutional lattice sites. Such displacements may be caused by interstitial In, phase separation such as In clustering or interaction of In with defects. Due to the low sensitivity of RBS to Al and the superposition of the Al-signal with the Ga-signal from the buffer layers, it is at this point impossible to say if this disorder is present only on the In-sublattice or if it is also present on the Al-sublattice.

As another indicator to assess crystal quality the broadening of XRD curves was examined. Although this broadening is also influenced by the compositional gradients mentioned above, it gives additional information on defects, in particular dislocation densities. The broadening of the spots shown on the $(10\bar{1}5)$ RSMs of Fig. 1 shows that the crystal quality is better in the $Al_{1-x}In_xN$ film grown on the GaN template, compared to the $Al_{1-x}In_xN$ films grown on the ternary $Al_{1-y}Ga_yN$ templates, suggesting a higher density of structural defects in the latter. The same conclusion can be taken from XRD RC widths summarized in Table III for all templates and films. Broadening of RCs is typically associated with screw and mixed dislocations while pure edge dislocations only affect asymmetrical RCs when measured in skew symmetric symmetry [31]. Surface defects may also contribute to the broadening of the XRD curves [32].

The lateral fluctuations of crystal quality in the samples grown on ternary templates described above should be connected to the growth templates rather than to the growth conditions, since the latter were the same in all samples. In order to understand better the reasons for the different crystal qualities of the films, AFM and SEM images were taken of the templates as well as the final $Al_{1-x}In_xN$ films (Figs. 4 and 5). Morphology studies show that the GaN template is the smoothest (rms roughness of 0.2 nm) and rms roughness values then increase with decreasing GaN content in the templates (the B, C and D templates have rms roughness values of 1.58 nm, 3.19 nm, 4.34 nm, respectively). The values of rms roughness of the $Al_{1-y}Ga_yN$ templates and the $Al_{1-x}In_xN$ films are summarized in table III and Fig. 4 i). From the histogram in Fig. 4 i) it is clear that the $Al_{1-x}In_xN$ film roughness increases with the roughness of the growth template. Although it is difficult to establish a relation between macroscopic crystal quality provided by RBS and XRD and the templates' morphology, it is interesting to note that both the film's roughness and the $<\bar{2}113>$ minimum yield increase with decreasing GaN content of the template. The same tendency is seen for the (0004) symmetric and $(10\bar{1}4)$ asymmetric RC widths (Table III) which both increase with increasing film roughness. Note that the RC broadening due to alloy composition and instrumental resolution is negligible according to simulations with the LEPTOS code [33].

SEM images of the four $Al_{1-x}In_xN$ films in Fig. 5 a) show that the morphology of the samples is homogeneous and that no cracks have formed during growth. In agreement with the AFM results, SEM reveals a degradation of the surface with decreasing GaN content of the template. In particular, the pit density is seen to increase strongly (Fig. 5 b)).

Hexagonal pits were shown to be the main morphological defects in $Al_{1-x}In_xN$ and $In_{1-y}Ga_yN$ grown on GaN [34-36]. Typically these pits are terminating threading dislocations that have their origin in the buffer layer but high pit densities were also found in some samples grown on buffer layers with low dislocation densities [35]. For the latter case, Perillat-Merceroz et al. proposed kinetic roughening and subsequent hillock formation as the origin of the V-defects which form when hillocks reach a critical height to stabilise growth on inclined facets [35]. The

same authors propose further that the coalescence of V-defects in thick $Al_{1-x}In_xN$ layers can lead to higher or lower InN-content in the surface layers due to the distinct In incorporation occurring on the concave or convex shaped surfaces of the V-defects [35]. Similar observations have been made for V-pits caused by threading dislocations [37].

This model can help to explain the phase separation that commonly occurs at the surface of $Al_{1-x}In_xN$ films [3,4,5,37,38] even when other factors such as strain, dislocations and impurities can be neglected. In this study, a pronounced decrease of In-content in the surface layer is observed in the two films with the highest V-pit densities (films C and D) indeed pointing to an influence of V-pits on the composition at the surface of our samples. In fact, in our samples the effect of growth parameters and impurities can be discounted when examining the processes leading to pit-formation and compositional gradients since the layers were all grown simultaneously. Also strain should play a minor role since the measured strain values are low. In compressively strained $Al_{1-x-y}In_xGa_yN$ a critical strain of ~1% was suggested to be the limit for homogeneous In-incorporation; above this value layers start to relax and compositional gradients are observed [5]. Our films show much lower strain values (see Table II). Furthermore, XRD analysis suggests that, in the present case, dislocations may also play a minor role. In fact, film B shows a significantly lower pit-density than films C and D although XRD RC broadening (Table II) suggests similar dislocation densities for the three ternary templates and corresponding films.

In an attempt to explain our results, we therefore proceed with an adaptation of the above described model by Perillat-Merceroz et al. [35]. Since the growth parameters are identical for the four samples, V-pit formation due to kinetic effects can be neglected. Nevertheless, the AFM and SEM images suggest that an increased roughness of the growth template promotes the formation of V-pits. We therefore conclude that this roughness may lead to preferential growth on inclined facets when 3D surface features reach a critical height, giving rise to V-defects when these growth fronts coalesce and explaining the decreasing In-incorporation close to the surface. V-pits correlated with dislocations may further contribute to the observed compositional gradients in samples B, C and D.

4. Conclusions

Near lattice matched $Al_{1-x}In_xN$ thin films were successfully grown on $Al_{1-y}Ga_yN$ templates with different GaN contents (y=1, ~0.93, ~0.86 and ~0.69). The MOCVD growth protocol allowed $Al_{1-x}In_xN$ layers to be grown simultaneously under the same global reactor conditions on de-oxidised template layers of different compositions, in a manner not possible when $Al_{1-x}In_xN$ is grown on a $Al_{1-y}Ga_yN$ layer of a single composition grown previously in the same deposition run. The compositional, structural and morphological properties of the resulting layers were studied. The highest quality was achieved for growth on the GaN template; this was attributed to its superior structural and morphological quality. $Al_{1-x}In_xN$ film grows pseudomorphically on GaN with an homogeneous composition profile and features low RBS/C minimum yields and a smooth surface. The $Al_{1-x}In_xN$ films grown on ternary templates have higher rms roughness values compared to that grown on the GaN buffer layer. The roughness is seen to increase with decreasing GaN content on account of the increasing roughness of the templates. An increasing density of surface pits, crystal quality fluctuations and compositional gradients are

observed in rough samples. These results indicate that the template quality does not only influence crystal quality and morphology but also the phase homogeneity of the $Al_{1-x}In_xN$ films. We suggest that high surface roughness promotes the formation of V-pits due to the preferential growth on side facets of the 3D surface structures and subsequent coalescence of these growth fronts. Compositional gradients can then be explained based on the distinct In-incorporation on the inclined facets of V-pits reported in the literature.

ACKNOWLEDGMENTS

Funding by FCT Portugal grants PTDC/FIS/65233/2006 and PTDC/FIS-NAN/0973/2012 and by the UK EPSRC grant EP/I029141/1 is gratefully acknowledged. KL thanks FCT for her grant as "Investigador FCT" and SM for his PhD Grant No. SFRH/BD/45774/2008 and post-doc grants under the Project NORTE-07-0124-FEDER-000070 and FCT No. SFRH/BPD/98738/2013.

References

[1] B. Gil (ed.), III-Nitride Semiconductors and their Modern Devices (Series on Semiconductor Science and Technology 18), Oxford University Press, ISBN 978–0–19–968172–3 (2013).

[2] S. Pereira, M. R. Correia, E. Pereira, K. P. O'Donnell, C. Trager-Cowan, F. Sweeney, E. Alves, Phys. Rev. B **64**, 205311 (2001).

[3] K. Lorenz, N. Franco, E. Alves, S. Pereira, I. M. Watson, R. W. Martin, K. P. O'Donnell, J. Cryst. Growth **310**, 4058 (2008).

[4] A. Redondo-Cubero, K. Lorenz, R. Gago, N. Franco, M-A di Forte Poisson, E. Alves, E. Muñoz, J. Phys. D: Appl. Phys. **43**, 055406 (2010).

[5] B. Reuters, M. Finken, A. Willie, B. Holländer, M. Heuken, H. Kalisch, A. Vescan, J. Appl. Phys. **12**, 093524 (2012).

[6] R. Butté, J-F Carlin, E. Feltin, M. Gonschorek, S. Nicolay, G. Christmann, D. Simeonov, A. Castiglia, J. Dorsaz, H. J., Buehlmann, S. Christopoulos, G. Baldassarri Höger von Högersthal, A. J. D. Grundy, M. Mosca, C. Pinquier, M. A. Py, F. Demangeot, J. Frandon, P. G. Lagoudakis, J. J. Baumberg, N. Grandjean, J. Phys. D: Appl. Phys. **40**, 6328 (2007).

[7] L. Vegard, Zeitschrift für Physik **5**, 17 (1921).

[8] D. Dadgar, F. Schulze, J. Bläsing, A. Diez, A. Krost, M. Neuburger, E. Kohn, I. Daumiller, M. Kunze, Appl. Phys. Lett. 85, 5400 (2004).

[9] M. Gonschorek, J. -F. Carlin, E. Feltin, M. A. Py, N. Grandjean, Appl. Phys. Lett. **89** 062106 (2006).

[10] K. Lorenz, N. Franco, E. Alves, I. M. Watson, R. W. Martin, K. P. O'Donnell, Phys. Rev. Lett. **97**, 085501 (2006).

[11] H. P. D. Schenk, M. Nemoz, M. Korytov, P. Vennéguès, A. D. Dräger, A. Hangleiter, Appl. Phys. Lett. **93**, 081116 (2008).

[12] C. Hums, J. Bläsing, A. Dadgar, A. Diez, T. Hempel, J. Christen, A. Krost, K. Lorenz, E. Alves, Appl. Phys. Lett. **90**, 022105 (2007).

[13] T. C. Sadler, M. J. Kappers, R. A. Oliver, Phys. Stat. Sol. C **6**, S666 (2009).

[14] Ž. Gacevic, S. Fernández-Garrido, J. M. Rebled, S. Estradé, F. Peiró, E. Calleja, Appl. Phys. Lett. **99**, 031103 (2011).

[15] M. Miyoshi, Y. Kuraoka, M. Tanaka, T. Egawa, Appl. Phys. Express **1**, 081102 (2008).

[16] E. Feltin, J.-F. Carlin, J. Dorsaz, G. Christmann, R. Butté, M. Laügt, M. Ilegems, N. Grandjean, Appl. Phys. Lett. 88, 051108 (2006).

[17] N. P. Barradas, C. Jeynes, Nucl. Instrum. Methods Phys. Res. B **266**, 1875 (2008).

[18] N. Herres, L. Kirste, H. Obloh, K, Köhler, J. Wagner, P. Koidl, Mat. Sci. and Eng. B **91-92**, 425 (2002).

[19] M. Tanaka, S. Nakahata, K. Sogabe, H. Nakata, M. Tabioka, Jpn. J. Appl. Phys. **36**, L1062 (1997).

[20] M. Yamaguchi, T. Yagi, T. Sota, T. Deguchi, K. Shimada, S. Nakamura, J. Appl. Phys. **85**, 8502 (1999).

[21] W. Paszkowicz, R. Cerny, R. Krukowski, Powder Diffr. **18**, 114 (2003).

[22] A. F. Wright, J. Appl. Phys. **82**, 2833 (1997).

[23] A. U. Sheleg, V. A. Savastenko, Izv. Akad. Nauk SSSR, Neorg. Mater. **15**, 1598 (1979).

[24] M.-Y. Xie, F. Tasnádi, I. A. Abrikosov, L. Hultman, V. Darakchieva, Phys. Rev. B **86**, 155310 (2012).

[25] F. M. Morales, J. M. Garcia, B. Reuters, H. Kalisch, A. Vescan, J. Phys. D: Appl. Phys. **46**, 245502 (2013).

[26] W. Jiao, W. Kong, J. Li, K. Collar, T. -H. Kim, A. S. Brown, Appl. Phys. Lett. **103**, 162102 (2013).

[27] J. Zhu, F. Liu, G. B. Stringfellow, S. -H. Wei, Phys. Rev. Lett. **105**, 195503 (2010).

[28] K. Lorenz, S. Magalhães, N. Franco, N. P. Barradas, V. Darakchieva, E. Alves, S. Pereira, M. R. Correia, F. Munnik, R. W. Martin, K. P. O'Donnell, I. M. Watson, Phys. Stat. Solidi B **247**, 1740 (2010).

[29] W. D. Nix and B. M. Clemens, J. Mater. Res. **14**, 3467 (1999).

[30] T. Ive, O. Brandt, X. Kong, A. Trampert, K. H. Ploog, Phys. Rev. B **78**, 035311 (2008).

[31] Y. J. Sun, O. Brandt, T. Y. Liu, A. Trampert, K. H. Ploog, J. Bläsing, A. Krost. Appl. Phys. Lett., Vol. 81, 4928, (2002).

[32] M. A. Moram, C. F. Johnston, J. L. Hollander, M. J. Kappers, C. J. Humphreys, J. Appl. Phys. **105**, 113501 (2009).

[33] Leptos V.4, Bruker AXS (2006).

[34] A. Vilalta-Clemente, M. Morales, M. P. Chauvat, Y. A-R. Dasilva, M. A. Poisson, M. Heuken, C. Giesen, P. Ruterana, Proc. of SPIE **7602**, 76020K-1 (2010).

[35] G. Perillat-Merceroz, G. Cosendey, J-F. Carlin, R. Butté, N. Grandjean, J. Appl. Phys. **113**, 063506 (2013).

[36] P. Vennéguès, B. S. Diaby, H. K.-Chaveau, L. Bodiou, H. P. D. Schenk, E. Frayssinet, R. W: Martin, I. M. Watson, J. Cryst. Growth **353**, 108 (2012).

[37] Q. Y. Wei, T. Li, Y. Huang, J. Y. Huang, Z. T. Chen, T. Egawa, F. A. Ponce, Appl. Phys. Lett. **100**, 092101 (2012).

[38] V. Darakchieva, M. Beckers, M.-Y. Xie, L. Hultman, B. Monemar, J.-F.Carlin, E. Feltin, M. Gonschorek, N. Grandjean, J. Appl. Phys. **103**, 103513 (2008).

Figure captions

Figure 1 a)-d): Reciprocal space maps around the $Al_{1-y}Ga_yN$ and $Al_{1-x}In_xN$ $(10\bar{1}5)$ reciprocal lattice point of the analysed samples.

Figure 2: 1.2 MeV He^+ random RBS spectra and fits of samples A, B, C and D. The In-signal between channels ~600 and 750 shows the variation of ~1% in the InN content with depth for sample B and ~5% for samples C and D. The $Al_{1-x}In_xN$ composition of sample A is uniform with depth (flat plateau of the In-signal). The spectra were shifted vertically for clarity.

Figure 3: 2 MeV He^+ random (open symbols) and <0001> aligned (filled symbols) RBS/C spectra of a) template B ($Al_{0.071}Ga_{0.929}N$) and b) film B ($Al_{0.833}In_{0.167}N$) acquired at three sample spots: wafer centre, middle of the sample strip and wafer edge. The Ga and In minimum yields for the three measured positions are given.

Figure 4: a-d) AFM images of the $Al_{1-x}In_xN$ films A, B, C, D. e-h) AFM images of templates A, B, C, D. i) rms roughness histogram of the $Al_{1-y}Ga_yN$ templates (filled black rectangles) and $Al_{1-x}In_xN$ films (open rectangles).

Figure 5: a) Secondary electron images of $Al_{1-x}In_xN$ films A, B, C and D. b) pit densities found in $Al_{1-x}In_xN$ films A, B, C and D extracted from the SE images.

Fig. 1

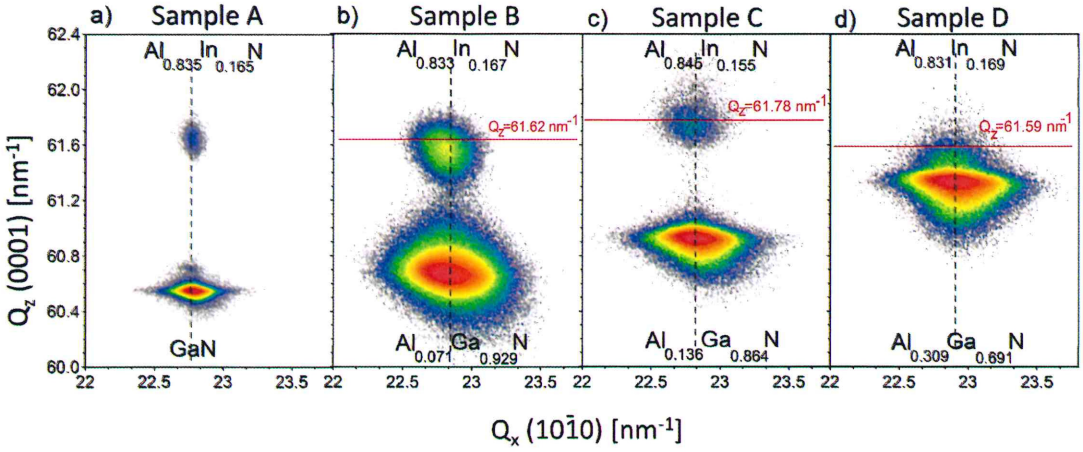
a) Sample A
b) Sample B
c) Sample C
d) Sample D
Al0.835 In 0.165 N
Al0.833 In 0.167 N
Al0.845 In 0.155 N
Al0.831 In 0.169 N
Qz=61.62 nm-1
Qz=61.78 nm-1
Qz=61.59 nm-1
GaN
Al0.071 Ga 0.929 N
Al0.136 Ga 0.864 N
Al0.309 Ga 0.691 N
Qz (0001) [nm-1]
Qx (10$\bar{1}$0) [nm-1]

Fig. 2

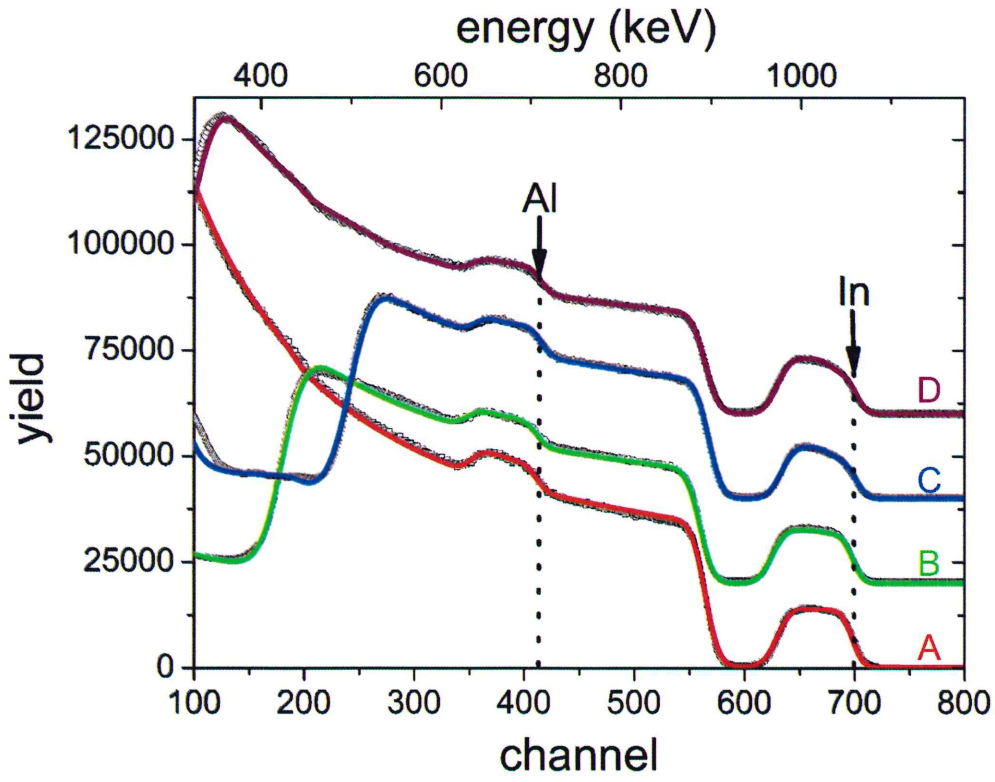
energy (keV)
yield
channel
Al
In
D
C
B
A

Fig. 3

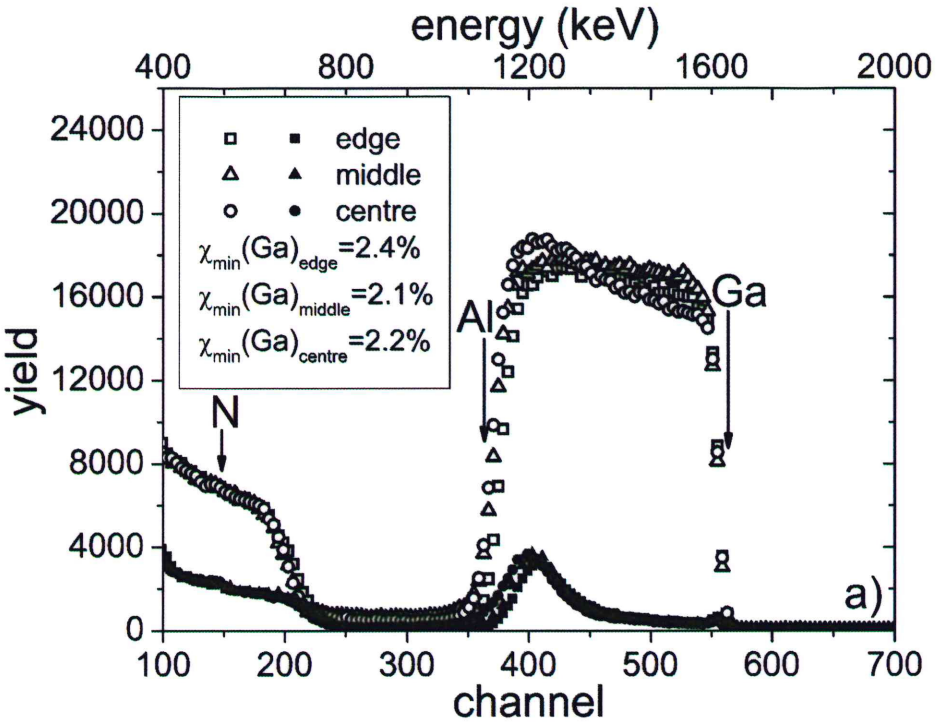
energy (keV)
400
800
1200
1600
2000
24000
20000
16000
12000
8000
4000
0
yield
edge
middle
centre
$\chi_{min}(Ga)_{edge}$=2.4%
$\chi_{min}(Ga)_{middle}$=2.1%
$\chi_{min}(Ga)_{centre}$=2.2%
N
Al
Ga
a)
100
200
300
400
500
600
700
channel

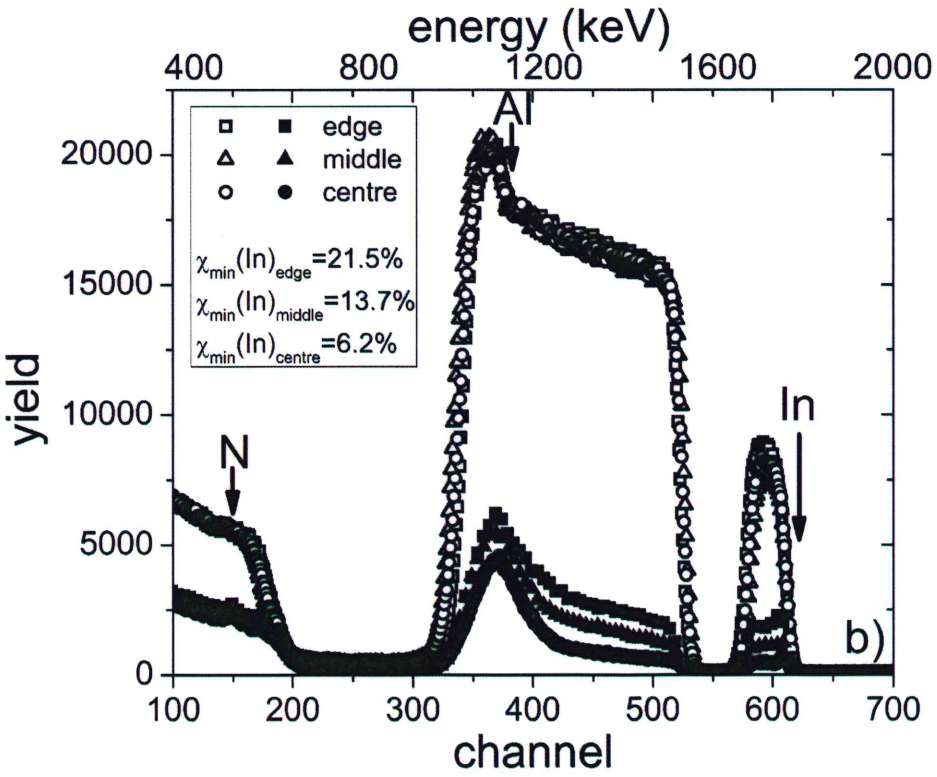
energy (keV)
400
800
1200
1600
2000
20000
15000
10000
5000
0
yield
edge
middle
centre
$\chi_{min}(In)_{edge}$=21.5%
$\chi_{min}(In)_{middle}$=13.7%
$\chi_{min}(In)_{centre}$=6.2%
N
Al
In
b)
100
200
300
400
500
600
700
channel

Fig. 4

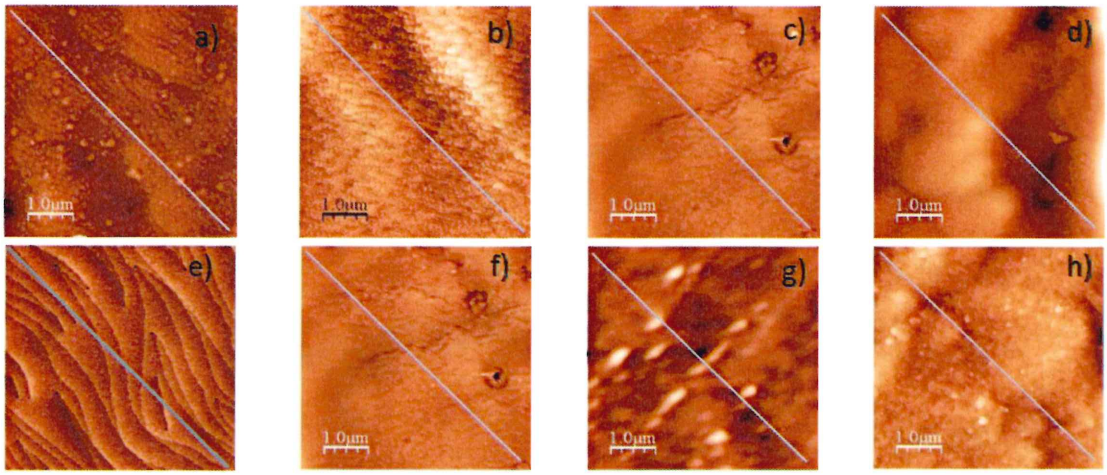
a)
b)
c)
d)
e)
f)
g)
h)
1.0μm

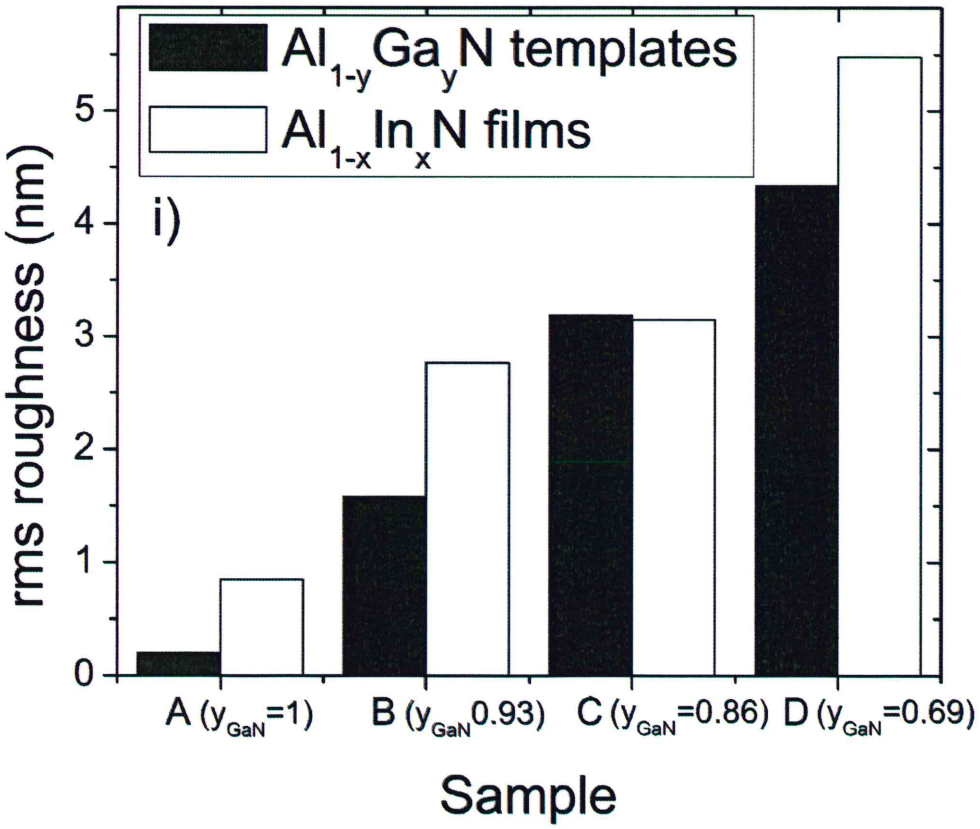
Al1-yGayN templates
Al1-xInxN films
i)
rms roughness (nm)
0
1
2
3
4
5
A (yGaN=1)
B (yGaN0.93)
C (yGaN=0.86)
D (yGaN=0.69)
Sample

Fig. 5

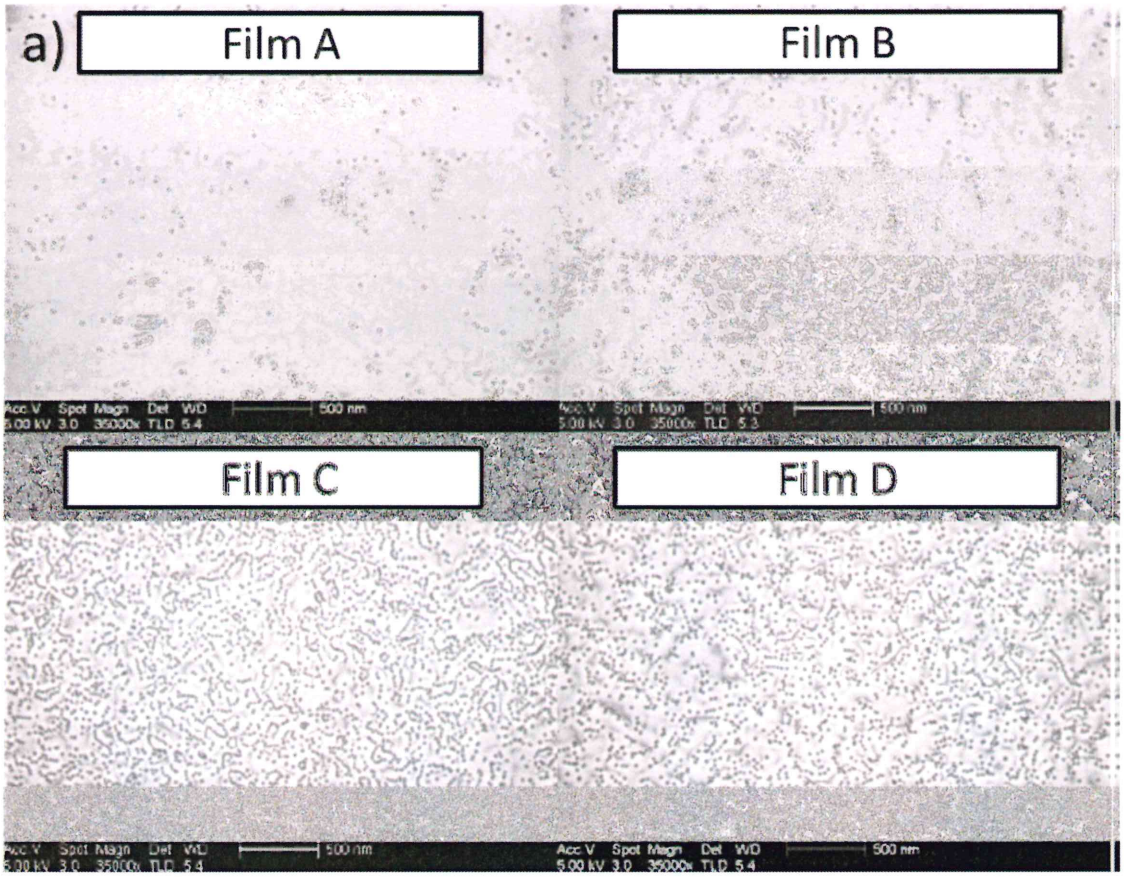
a)
Film A
Film B
Film C
Film D

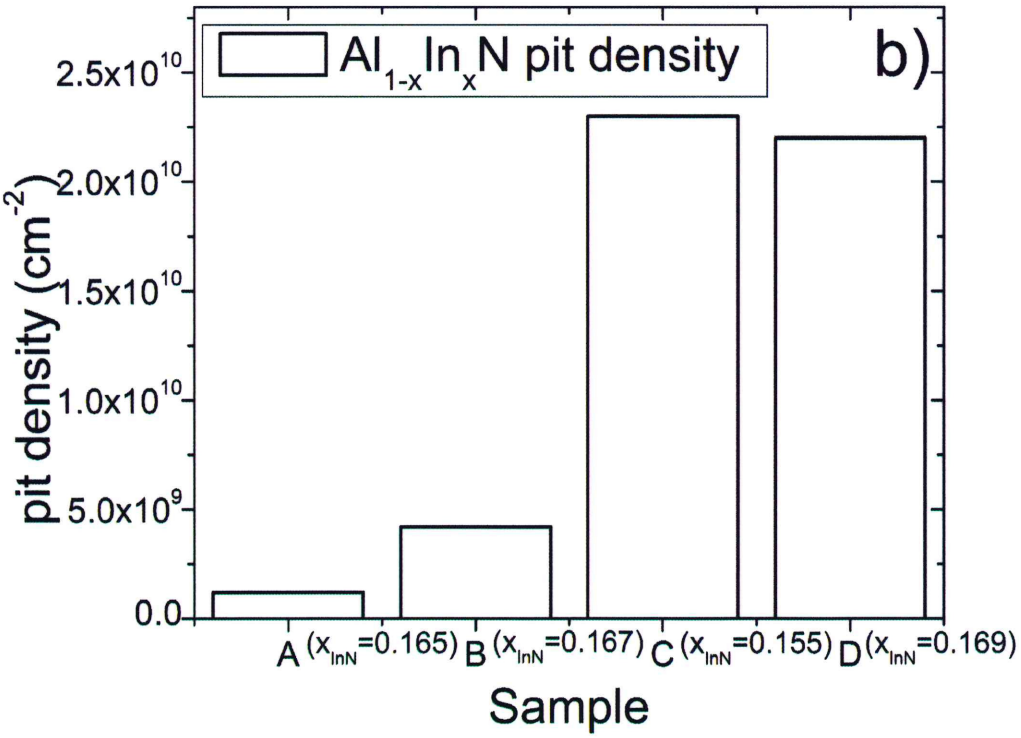
b)
Al1-xInxN pit density
pit density (cm-2)
2.5x10^10
2.0x10^10
1.5x10^10
1.0x10^10
5.0x10^9
0.0
A (xInN=0.165)
B (xInN=0.167)
C (xInN=0.155)
D (xInN=0.169)
Sample

INTENTIONALLY BLANK

Table I: Relaxed lattice parameters of the binaries AlN, GaN and InN and stiffness coefficients used in this work.

Binary	a_0 (Å)	c_0 (Å)	C_{13} (GPa)	C_{33} (GPa)
AlN	3.1110 [19]	4.9800 [19]	99 [21]	389 [21]
GaN	3.1896 [20]	5.1855 [20]	103 [22]	405 [22]
InN	3.5377 [21]	5.7037 [21]	121 [23]	182 [23]

Table II: Measured a and c lattice parameters of the $Al_{1-y}Ga_yN$ templates and $Al_{1-x}In_xN$ films; the templates' molar GaN fraction yGaN and the $Al_{1-x}In_xN$ films' molar InN fraction xInN measured by XRD; the lattice parameters a_0 and c_0 for a relaxed ternary with the corresponding composition and the InN molar fraction xInN LM for which lattice-matching (LM) to the corresponding template would occur; the parallel $\varepsilon^{||}$ and perpendicular $\varepsilon^{\perp}$ deformations.

Sample #	Template	a parameter (Å)	c parameter (Å)	yGaN	a_0 (Å)	c_0 (Å)	$\varepsilon^{||}$ (%)	$\varepsilon^{\perp}$(%)	
A	GaN	3.185±0.001	5.189±0.001	1	3.1896	5.1855	-0.144	0.067	
B	$Al_{0.071}Ga_{0.929}N$	3.177±0.001	5.177±0.001	0.929±0.002	3.184	5.171	-0.220	0.116	
C	$Al_{0.136}Ga_{0.864}N$	3.178±0.002	5.158±0.001	0.864±0.003	3.179	5.158	-0.031	0.000	
D	$Al_{0.309}Ga_{0.691}N$	3.166±0.002	5.121±0.002	0.691±0.004	3.165	5.122	0.032	-0.020	
Sample #	Film	a parameter (Å)	c parameter (Å)	xInN (XRD)	a_0 (Å)	c_0 (Å)	$\varepsilon^{||}$ (%)	$\varepsilon^{\perp}$(%)	xInN LM
A	$Al_{0.835}In_{0.165}N$	3.186±0.001	5.096±0.001	0.165±0.001	3.181	5.099	0.157	-0.059	0.173
B	$Al_{0.833}In_{0.167}N$	3.180±0.003	5.102±0.001	0.167±0.002	3.182	5.101	-0.063	0.020	0.154
C	$Al_{0.845}In_{0.155}N$	3.184±0.002	5.086±0.001	0.155±0.002	3.177	5.092	0.220	-0.118	0.157
D	$Al_{0.831}In_{0.169}N$	3.172±0.005	5.112±0.005	0.169±0.011	3.183	5.102	-0.346	0.196	0.130

Table III: Indicators of templates and films that define the crystal quality and morphology: measured and simulated RC FWHM (the values correspond to an average over many measurements at different positions across the wafer radius and their standard deviation) of the $(10\bar{1}4)$ and (0004) reflections, minimum yields χ_{min} (measured in the wafer centre (c), middle of sample slice (m) and wafer edge (e)) and rms roughness.

Sample #	Template	$(10\bar{1}4)$ FWHM exp, theoretical (deg)		(0004) FWHM exp, theoretical (deg)		χ_{min}(Ga) <0001> (%)	χ_{min}(Ga) <$\bar{2}$113> (%)	rms roughness (nm)
A	GaN	0.065±0.002	0.0164	0.089±0.007	0.0216	1.7±0.1 (m)	2.7±0.1 (m)	0.2
B	$Al_{0.071}Ga_{0.929}N$	0.234±0.010	0.0164	0.290±0.001	0.0215	(2.2 (c) ; 2.1 (m) ; 2.4 (e)) ±0.2	8.0±0.1 (m)	1.58
C	$Al_{0.136}Ga_{0.864}N$	0.191±0.008	0.0164	0.224±0.010	0.0215	2.9±0.1(m)	6.1±0.1 (m)	3.19
D	$Al_{0.309}Ga_{0.691}N$	0.227±0.007	0.0164	0.283±0.013	0.0213	2.4±0.1 (m)	5.6±0.1 (m)	4.34
Sample #	Film	(10-14) FWHM exp, theoretical (deg)		(0004) FWHM exp, theoretical (deg)		χ_{min}(In) <0001> (%)	χ_{min}(In) <-2113> (%)	rms roughness (nm)
A	$Al_{0.835}In_{0.165}N$	0.255±0.007	0.0679	0.182±0.005	0.0457	(4.5 (c) ; 4.4 (m) ; 4.5 (e)) ±0.2	8.2±0.2 (m)	0.85
B	$Al_{0.833}In_{0.167}N$	0.357±0.030	0.0680	0.312±0.018	0.0458	(6.2 (c) ; 13.7 (m) ; 21.5 (e))±0.2	23.2±0.4 (m)	2.77
C	$Al_{0.845}In_{0.155}N$	0.372±0.015	0.0678	0.352±0.013	0.0457	(11.6 (c) ; 10.4 (m))±0.2	30.5±0.5 (m)	3.15
D	$Al_{0.831}In_{0.169}N$	----	0.0680	----	0.0459	(9.7 (c) ; 10.2 (m) ; 15.1 (e))±0.1	37.2±0.5 (m)	5.48